08,10

Topological dendrite structures with regulated micro-nanomodification with controlled electrophysical characteristics in experiment with laser ablation from a hard surface of stainless steel

© D.D. Tumarkina, A.F. Lelekova, K.S. Khorkov, D.N. Buharov, S.M. Arakelian

Federal State Budget Educational Institution
of Higher Education Vladimir State University named after Alexander and Nikolay Stoletovs
Vladimir, Russia

E-mail: tumarkina.darya@mail.ru

Received June 1, 2025
Revised August 6, 2025
Accepted August 19, 2025

Topological dendritic structures with controlled micro/nanomodification on the surface, obtained in different schemes of laser experiment with stainless steel AISI 304, are investigated. The synthesis of such structures and the methodology for measuring their characteristics in certain configurations on the surface of steels with a high-entropy composition are considered. The measurements were conducted using scanning tunneling/atomic force microscopy and Raman spectroscopy. Model calculations of fractal dimensions have been performed for the obtained heterogeneous topological surface objects in samples with a controlled dendritic fractal structure. The paper discusses the electrophysics of such structures and their possible applications based on the results of the conducted research. The paper presents the results of experiments on measuring the dependencies for the current-voltage characteristics of the micro/nanostructured surface of AISI 304 stainless steel samples modified by laser exposure.

Keywords: thin films, solid surface, laser exposure, micro-nanostructures, dendrite configurations, fractal dimension, high-entropy compounds with controlled topology, phase transformations.

DOI: 10.61011/PSS.2025.09.62360.153-25

1. Introduction

Materials with surface 2D-nanostructures in complexes of metals and semiconductors are a fundamental field for modern physics of solid-body phase states, which is promising for various applications [1–6]. These micro-nanosystems of the cluster type, which have various configurations and topologies regulated during their synthesis, originate specific localized states with controlled functional characteristics, in particular, electrophysical ones. It enables using this base for developing various devices of micro-nanoelectronics and photonics on new physical principles [4–6].

For regulated production of these structures, experimental laser diagrams are widely used, which include quite promising technologies of laser ablation of a solid-body surface with ejection of a substance under laser impact in its various modifications (cf. [7,8]). The laser ablation effect depends on a medium, in which a target is arranged, in particular, in liquid. Here, extreme conditions may occur, at which, for example, graphite transits into diamond-like structures at relatively low-power laser radiation due to local hydrodynamic shock processes in a laser beam focus in liquid (see [5,9,10]).

We are talking about synthesized thin-layer micro-nanostructures on the sample surface, which originate under direct impact of laser pulses and beams on its material in various modes. For example, it can happen with taking into account deposition and condensation of ablation products to the sample surface from a gas-vapor phase under thermal impact by a sequence of laser pulses and beams as well as a result of a two-stage process — production of nanoparticles in a colloid during laser ablation of the material in liquid with the subsequent deposition from the colloid to a solid substrate in a controlled way when scanning with the laser beam within a volume of the colloid. At the same time, specifics of physics of phenomena during deposition of objects to the solid surface of the substrate is determined by a degree of roughness of the substrate and thermal conductivity of its material. When considering electrophysics of these devices, the first things to be investigated are processes of controlling their conductance in a dependence on a configuration of the surface micro-nanotopology.

Transmission of electric current in structures, where conducting and non-conducting local areas alternate on the surface, can be described within the framework of representations of a percolation theory [4,11] that is applicable for this class of objects and they can be related to topological insulators [12].

Such cluster structures are of the highest interest for application in the thin-film metal systems of the type of ohmic and barrier contacts, thin-film resistors, capacitors as well as when transferring charge carriers through contact areas, etc. At the same time, single-electron quantum modes

can be realized to have mode switching in the same way as in a various type of diodes, in particular, tunnel ones (cf. [4,11,12]).

Percolation effects in these metal films are basically considered with studying the influence of transverse (perpendicular to the substrate plane) sizes (thicknesses) on their conductance. However, electrophysics of this kind of discrete topological structures with nonuniformities (dendrites of a micro-nanometer size) depends on their fractal geometry (cf. [12–14]).

These problems are investigated by us in the present study for an ensemble of dendrites on the surface of the AISI 304 stainless steel, which are experimentally synthesized as a result of two-pulse laser ablation (cf. [15]). The obtained results can be considered also by analogy as for a solid-state material of a high-entropy alloy (HEA) — with at least 5 chemical elements in the composition at their approximately identical percent concentration, cf. [16,17].

In our case, the emphasis is placed on controllability of functional characteristics of these structures during temperature phase transformations with variation of symmetry of crystal lattices [18,19]. We will shortly discuss them here in a laser-thermodynamic aspect together with various modes of subsequent processes (which are competitive for multipulse laser radiation) of heating and cooling the stainless steel material under laser impact on it in the atmosphere surrounding the sample.

The main subject of research in the present article is an experimentally detected explicit dependence of the electrophysical characteristics — current-voltage characteristics (I-V curves) — on a configuration of the laser-induced topology on the stainless steel surface, which occurs at various modes of laser ablation.

2. Methods and approaches — basic physical principles

2.1. Thermodynamic phase transformations under laser impact on the solid surface

The laser ablation process means that a liquid phase that is formed during laser melting is ejected from the surface similar to a process of highly-efficient gas-dynamic evaporation. It is a non-stationary hydrodynamic process with a certain velocity of motion of a boundary of the solid body → liquid phase transition, which can demonstrate an explosive exponential growth (cf. [8,20]) that is accompanied by surface deformation with taking into account recoil pressure and by formation of a crater in a melt bath.

Thermodynamically, similar phenomena can be related to a specific section of complex-system thermodynamics, which deals with phase transformations under conditions of implementation of nonlinear non-equilibrium processes (cf., for example, [20]). However, we will consider only the very fact of controlled formation and recording of heterogeneous topological structures of the dendritic type on the surface of the stainless steel in the laser experiment.

When the melt bath is formed under laser impact, we will be interested in formation of a different orientation of the dendritic objects with a fractal structure on the target surface as a result of occurred space-heterogeneous laser ablation with successive laser heating and subsequent cooling of the medium (cf. [13,15]). It is also necessary to take into account interaction of incident laser radiation with the substance when it is ejected during ablation. Fine-needle structures that are originated at this (with presence of martensite and residual austenite, similar to crystallographic phase modifications of metals) [16–18] are determined by non-equilibrium rates of heating and cooling in a dependence on the laser radiation modes with heterogeneity of a process of crystallization over the surface of the material (cf. [20,21]).

2.2. Specific features of laser impact on the HEA system

The above-listed reasoning was referred to the material that is homogeneous in the elemental chemical composition, whereas the HEA requires comprehensive analysis with taking into account effects of thermal diffusion for different components of the alloy and taking into consideration that a maximum of the temperature of laser heating is shifted into a less heat-conducting material to a greater extent the higher duration of the laser pulse [20].

In this aspect, synthesis of the micro-nanoscale surface structures on the solid-body surface is interesting and a separate area of research with the dendritic structures is included here. In this field, laser impact on the target during laser ablation with subsequent deposition of the ablation products to its surface with controlled production of the configuration-pre-defined topology of a certain scale has already led to some significant results (see, for example, [6,14]).

In these tasks, a mechanism of this impact with implementation of the topological phase transitions is based on thermophysical processes under laser radiation of the samples. Therefore, thermodynamics of these processes is crucial for investigating modification of the required functional characteristics, in particular, electric ones. At the same time, it is important to maintain a sequence of impact by laser pulses with different parameters, with a certain delay between them depending on constitutive parameters of the medium and its environment. It is related to effects of preliminary submelting with subsequent thermal diffusion of particles of different elements, which result in formation of dendrites with a regulated configuration on the surface of the material (cf. [13–15]).

For the considered synthesized structure configurations of a pre-defined type on the solid-body surface, under conditions of the laser experiment we can talk about the specific area of thermodynamics — laser thermodynamics [5,22]. We mean the processes when it is possible to induce

various phase states of the medium in subsurface layers in a regulated way at the various modes of laser impact on the solid-body surface with variation of the laser radiation characteristics (with its energy and time parameters selected) as a result of the non-equilibrium thermodynamic processes. At the same time, it is essential that the local temperature for heterogeneous areas of the dendritic/fractal type can significantly differ from the average heating temperature of the sample, thereby resulting in local melting of the material in these areas under impact of laser radiation, which is even relatively weak in terms of energy, on the medium (cf. [6]).

For simplicity and certainty, we used two-pulse laser ablation for producing dendrites in the thin layers on the surface of a target substrate of the thickness of 1 mm, which is made of AISI 304 stainless steel and has the following composition of the chemical elements (in wt.%): C — up to 0.08; Cr — 17.5–20; Fe — 66.345–74; Mn — up to 2; Ni — 8–11; P — up to 0.045; S — up to 0.03; Cu — up to 1 [13,15,23].

We made a number of experiments with this material under two-pulse impact in the M-pulse model with selected duration (cf. [11]). In the area of impact of the laser beam, the first laser pulse was implementing a substance pre-melting mode, and along with it oxidative destruction occurred at slow spontaneous cooling within the temperature interval from ~ 1860 (an estimate of start of melting of one phase) to 1067 K (a start of the subsequent phase transformation) [16,17] upon completion of impact of the laser pulse. This effect is similar to a process of intercrystalline corrosion of stainless steel (cf. [16,17,24]). However, direct measurements in a real time scale can be made by a brightness temperature in an original procedure using an additional laser monitor (see [5]), which we used in our other experiments during laser-induced synthesis of the allotropic phase of carbon — carbyne, in a carbon-containing material [9].

In this two-pulse format, the second laser pulse was creating the crystal structure of the dendrites under conditions of occurring natural cooling due to a time shift between two impacts of laser radiation on the surface of the sample and controllably forming the final configuration of the dendrites. Their structure and the specific features of the occurring non-linear non-equilibrium thermodynamic process were determined by a duration and a rate of cooling, which were adjusted when selecting parameters of the second laser pulse, upon completion of its effect the medium is quickly cooled [13,15,20].

In this diagram of two-pulse laser impact on the material at the total time of impact with durations of the laser pulse from 1 to 6 ms and at a respective density of the irradiation energy flux from 3.3 to $0.5 \cdot 10^6$ J/m^2/s, our performed studies of the thermophysical process resulted in a dependence of the temperature on the irradiated stainless steel with a temperature variation range from 335 to 1215 °C, respectively. We have obtained the given digital values when simulating distribution of a temperature field on the stainless steel substrate under conditions of a parabolic law of the temperature increase during laser irradiation of the target.

In a more general case, with achieving various thermodynamic modes, the process can be realized under impact of a sequence of laser pulses with their selected parameters (see, for example, [5]).

Without dwelling on our used model for analysis [13], we just note that laser heating results in an increase of entropy (cf. [25]), which in this case of complex compounds is entropy of mixing, and in synthesis of ceramic HEA perovskite with certain concentrations of the components. It is provided by selecting the heating temperature and the duration between the two pulses in this case for the stainless steel after a process of its oxidative destruction, which occurs, for example, in the air atmosphere. But, on the other hand, fast cooling upon completion of impact of the second laser pulse results in origination of thermodynamic states with chemical transformations, whose products include martensite with formation of the configurations of the dendrites. It is possible since martensite for the stainless steel is formed, as it is known, within the wide range of the temperatures (when its surface is overcooled from ~ 900 °C to the room temperature) [16,17].

A fundamental possibility of implementing control of the topology of the dendrites and their elemental composition is provided by selecting respective characteristics of impact in the laser experiment.

3. Results for the configurations of the laser-induced surface structures during the thermophysical processes and discussion

3.1. Synthesis of the micro-nanodendrites on the surface of the AISI 304 stainless steel

In our case, we have used laser impact in the air atmosphere on a pre-cleaned surface of the stainless steel with the following parameters in the laser experiment: radiation of the Nd:YAG-laser (of the CLW-50CTM type) with the radiation wavelength $\lambda = 1.06\,\mu$m; the two-pulse mode was realized as a M-shaped pulse with intervals between its two fragments 3 ms; the energy in the pulse was selected by us to be 10 or 12 J; the total duration of this combined laser pulse had a value of τ from ~ 6 to 12 ms with an increment of 2 ms; the diameter of a light spot in the laser radiation focus on the sample was ~ 1 mm. It resulted in origination of a modified layer of the thickness of ~ 20 nm on the sample with formation of the dendrites at the temperature of surface heating of the stainless steel up to 1860 K — as estimated according to the parabolic law of oxidation (cf. [13,14,23]). According to physics of the occurring phenomena, during laser ablation of the target surface not its initial state, but a selected ablation mode and a target structure after ablation are crucial, including with taking into account processes of reverse deposition of its

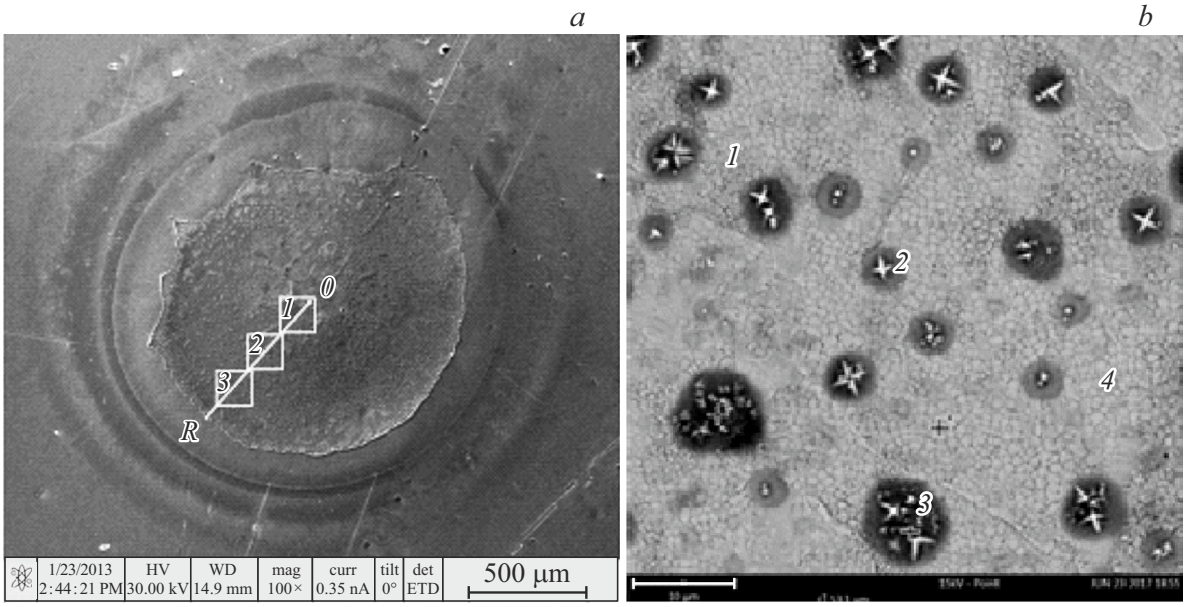

Figure 1. *a*) Area of laser impact with the M-pulse. Three zones *1*–*3* are shown: from the center of the focused laser beam (the zone 0) to the periphery (the zone *R*) of the laser beam with its impact on the surface. *b*) SEM-image of the zone *2* with arrangement of the dendrites on its surface (the digits denote points).

fragments to the surface. It is this factor that determines parameters of the appearing dendrites.

Caverns of the size 1×1 mm, which were formed on the sample surface in the laser impact zones, were first recorded in an optic digital microscope with revealing tempering colors that indicated that there was an oxide film on the surface of the material. Then, a scanning-electron microscope (SEM) was used to detect an area of propagation of the very dendrites, which were, inter alia, in the areas *1* and *3* shown in Figure 1. They were uniformly distributed, in particular, in the area *2* of the cavern (it is separately shown in Figure 1, *b*).

Besides, atomic force microscopy (AFM) was used to determine sizes of the dendrites (Figure 2). These parameters are estimated to result in tot following average values: a diameter of a circle circumscribed around the dendrite base is $2.7\,\mu$m, a dendrite height is $1.7\,\mu$m.

It was found by the results of the performed energy-dispersive analysis that the areas not processed by laser radiation were dominated by iron in the same way as in areas between the dendrites. A percentage of the components for this grade of the stainless steel was almost equalized in a location of single dendrites or their clusters after laser impact (see Table 1 with numbers of points designated in Figure 1, *b*).

The point *3* in Table 1 defines an area, in which the dendrites are clustered on the surface of the stainless steel.

We have also calculated a value of mixing entropy S_{diff} for this composition of the elements with an adiabatic process assumed, by a procedure that is specified in [15] for designated parameters of the laser thermodynamic process.

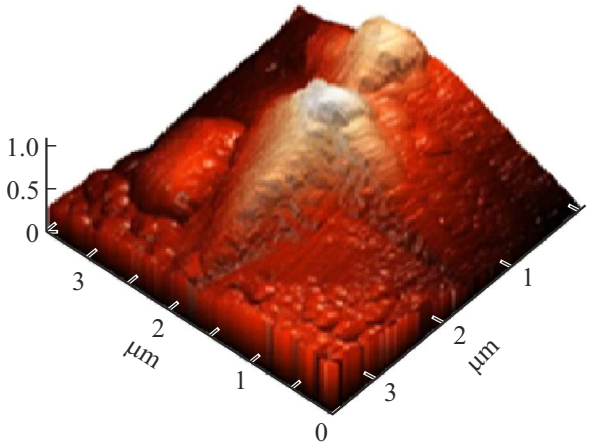

Figure 2. Parameters of a single dendrite on the AFM image.

The area of the cluster of the dendrites corresponds to maximum mixing entropy of components of the elements in the sample. Calculated distribution of mixing entropy S_{diff} in one of the zones on the surface of the sample is shown in Figure 3. Thus, it can be concluded that the surface of the sample has the high-entropy alloy with defects under the oxide film (cf. [15]).

A study of the thermodynamic conditions for producing these structures and our performed analysis demonstrated that the initial stage of laser impact could include synthesis of the structure with availability of heterogeneities and defects with a multi-element chemical composition of the high-entropy perovskite type (with the percentage of the

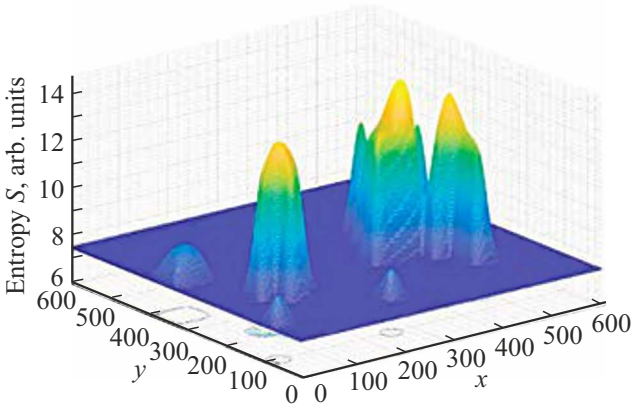

Figure 3. Calculated determination of mixing entropy S_{diff} over the surface of the sample in the area *3* in Figure 1, *a*.

Table 1. Values of the concentrations of the elements, which are averaged over 20 different measurements of the areas in various samples of the AISI 304 steel in the fixed points *1*–*4* on the surface of the sample after laser impact

No. of point	Portion of the chemical element, %						
	Fe	Cr	O	Ni	Mn	C	Σ
1	63.2	16.7	8.6	7.8	2.2	1.5	100
2	19.0	24.8	32.6	1.3	20.6	1.7	100
3	41.1	18.1	26.2	4.7	8.8	1.1	100
4	69.4	18.0	0	9.7	1.7	1.2	100

elements in our case: ∼ 9 % — C, ∼ 14 % — Cr, ∼ 9 % — Fe, ∼ 11 % — Mn, ∼ 11 % — Ni, ∼ 46 % — O). At the same time, the thermodynamic stages of the occurring processes under laser impact were reduced in terms of phase transitions (cf. [26]) to the following sequence: the stainless steel is transformed to become high-entropy perovskite, from which martensite is formed. We state this based on using results of the study [26] with taking into account our own studies of dynamic instabilities during laser ablation of the sample.

3.2. RS-spectrum of the dendrites on the surface of the AISI 304 stainless steel

Below is one example of our measured typical spectra of Raman scattering (RS) in inverse centimeters with intensity in units of photocounts for surfaces of some samples made of the AISI 304 stainless steel with the dendrites (only one of them is shown for brevity — Figure 4: they are almost identical for our studied samples). The configurations of the dendrites are obtained at laser impact parameters given in the previous paragraph. These spectra were compared by us with RS-spectra of bixbyite — ($Fe-Fe_2O_3$) from the RRUFF database [27] to show good match. At the same time, the measured spectra include a number of various lines of rotational and oscillatory resonances, whose shape and characteristics depend on sizes of surface heterogeneities — micro-nanoparticles.

It is clear from Figure 4 that strong Raman peaks (500 and 700 cm^{-1}) correspond to availability of the substance Fe_2O_3 (cf. [28]). At the same time, the surface profiles (for example, along the axis $0X$, Figure 3) have a similar relief in the different samples. These peaks in the spectra were observed in all the samples. Based on this, it can be believed that in addition to the phase transformation of perovskite into martensite, at the same time with it an iron oxide was formed on the dendrite surface due to evaporation of carbon in martensite out of a martensite lattice (cf. [29]).

In the oxide film formed on the surface of the dendrite during an oxidation-reduction reaction oxygen can appear from the oxide layer on the target or from air oxygen. As for lack of atoms of manganese, chromium, nickel in the spectrum of Figure 4, when digressing from its oscillatory nature, then it is possible to assume that they diffuse deep into the substrate, while carbon from molecules CO_2 likely arrives into the sample directly from atmospheric air. We again note that in a dependence on the laser ablation mode (energy parameters of affecting laser pulses and beams) a certain depth of modification of the target surface is realized.

Using measurements of Figure 4, means of confocal microscopy can be taken to rebuild a scanned surface of the sample. Then, the most intense peaks that correspond to Fe_2O_3 will be also determined by areas of arrangement of the dendrites along the substrate surface. Thus, indeed, it can be concluded that by the chemical composition the dendrites consist of the system Fe_2O_3.

It is of particular interest to evaluate a fractal dimension of such dendritic objects. Below, we briefly provide these results for similar measurements that have been also performed by us in the experiments with the chromium-vanadium steel by the same procedure of two-pulse ablation of its surface.

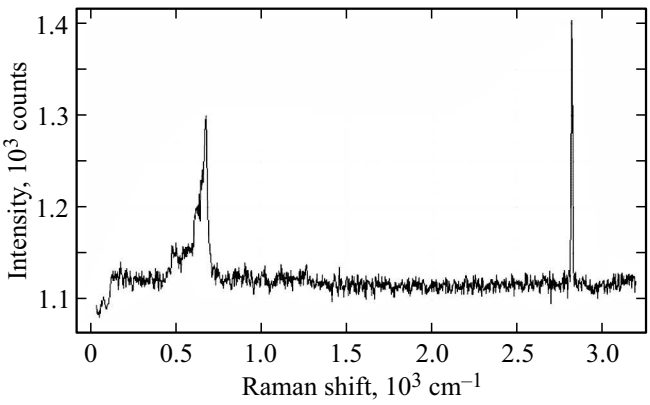

Figure 4. RS-spectrum obtained on one of the samples of the AISI 304 stainless steel with laser-synthesized dendrites on the surface of the solid sample.

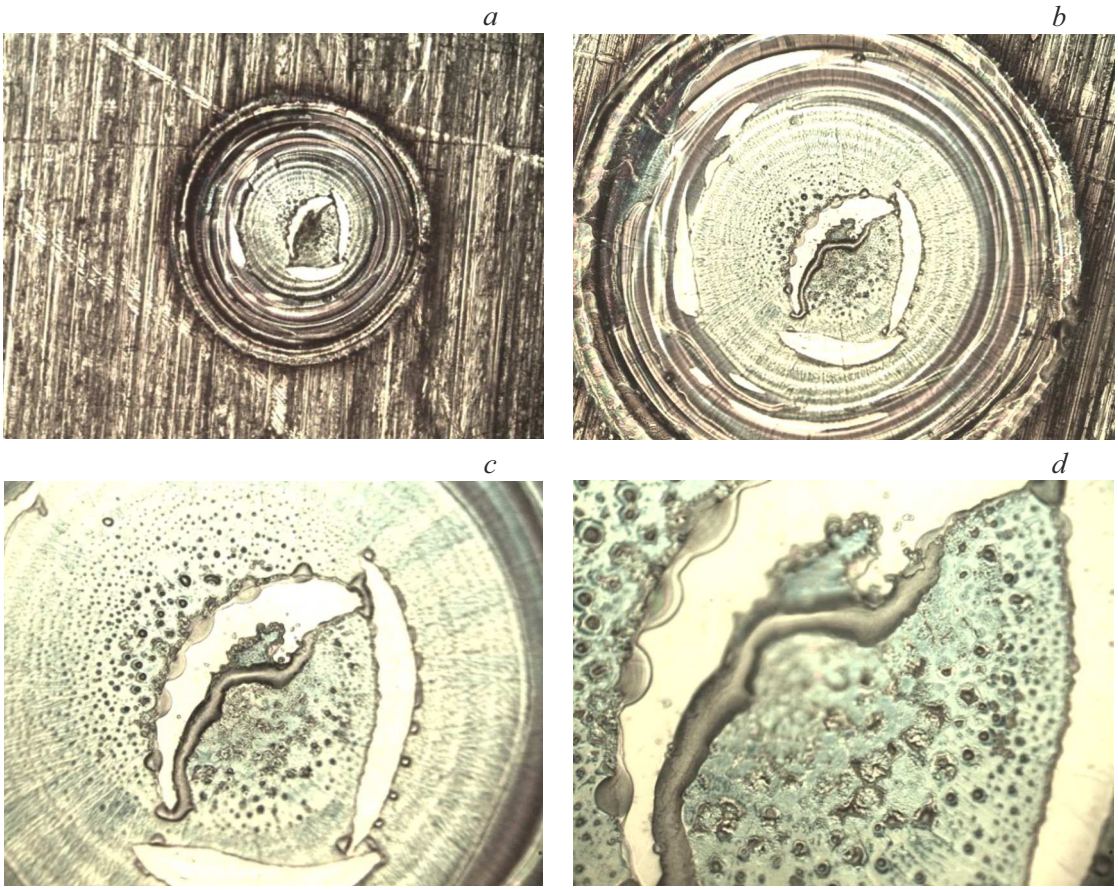

Figure 5. Optical microscopy of the laser-induced dendritic structure in the cavern on the surface of the stainless chromium-vanadium steel under different magnification: *a*) ×125; *b*) ×250; *c*) ×500; *d*) ×1000.

3.3. Evaluation of fractal dimension in the experiments with the chromium-vanadium type of the stainless steel

For the chromium-vanadium stainless steel, its chemical composition with the dendrites synthesized in our experiment under laser impact is shown in Table 2.

The structure of the produced surface in the laser-formed cavern after such laser impact, which is recorded by an optical microscope MKI-2M-1, is shown in Figure 5 and demonstrates that the surface really includes the dendritic objects.

Results of calculation of the fractal dimension for the various input parameters of the laser experiments with the chromium stainless steel are given below in Figure 6, *a* for the area on the image of the surface structure shown in Figure 6, *b*. At the same time, we used a calculation procedure (see [30]) in a format shown in Figure 6, *c*.

It is obtained that during two-pulse ablation in the format of the dependence (E, t), where E is a laser radiation energy, t is a duration of its pulse, for the formed dendrites in some different-composition substrates made of the stainless steel the fractal dimension had on average the same value of 1.9.

Table 2. Chemical composition of the dendrites for the chromium-vanadium stainless steel

Element	Percentage, %
Fe	81.9
Mn	0.3
V	0.2
Cu	0.1
Cr	17.0
Ti	0.2
Ni	0.1
C	0.2

It can be stated that based on implementation of the various values of the fractal dimension it is possible under laser impact to control in a pre-defined way the configuration of the appearing dendrites and to determine functional physical characteristics of the produced locally-heterogeneous solid-state objects.

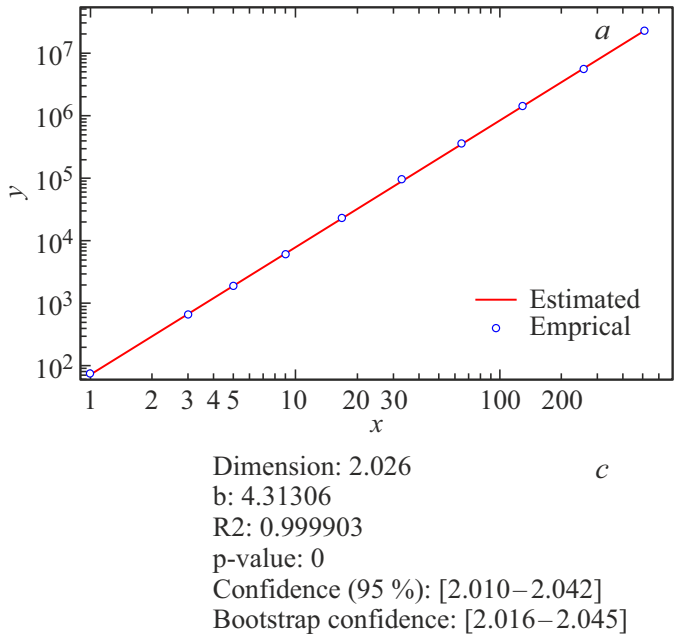

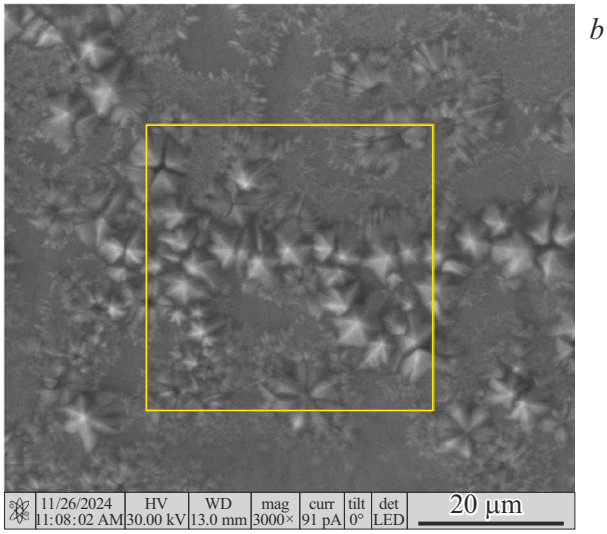

Figure 6. Conditions and results of calculation of fractal dimension for the chromium-vanadium steel after laser impact. *a*) The empirical curve is shown by circles, while the estimated model (a regression curve) is shown by a red line. *b*) SEM-image of the surface of the chromium-vanadium steel: a square is used to select an estimated area of fractals. *c*) Window with numerical results, with designations: „Dimension“ — fractal dimension, „b“ — a shift parameter in a selected model with space coordinates ($\log y = D\log x + b$), „R2“ — a coefficient of determination of regression, „p-value“ — regression significance (it shall be below 0.001), „Confidence“ — a confidence error, „Bootstrap confidence“ — a confidence error as a result of regression self-adjustment.

4. Electrophysics of the dendritic structures on the sample surface, which are synthesized in the laser experiment — I-V curves

In order to study the electrophysical properties of the considered surfaces with the laser-synthesized dendrites, their I-V curves were recorded. Measurement microcontacts to be energized were placed on the samples in various points of the surface with its respective scanning between selected local areas by means of a scanning tunnel microscope (STM) NTEGRA-Aura produced by NT-MDT, in the direct current mode at normal external conditions ($T = 295\,\mathrm{K}$) in a natural environment. Probably, it can be assumed that between a needle of the tunnel microscope as a microcontact on the sample surface and the very sample, to which the second microcontact is applied, electrons are tunneled in vacuum in our case. The I-V curves were taken within the range from $+1$ to $-1\,\mathrm{V}$. The measurements were averaged along 200 obtained data per one second in each point. For a selected set of parameters of laser processing of the surface, it was analyzed for our studied steel with selecting at least 100 points on the surface with subsequent statistical data processing. The results were automatically processed by means of respective software.

Figure 7 shows a setup for measuring the I-V curves. After laser impact, the sample with the dendritic structure in the caverns was placed on a movable optic table with

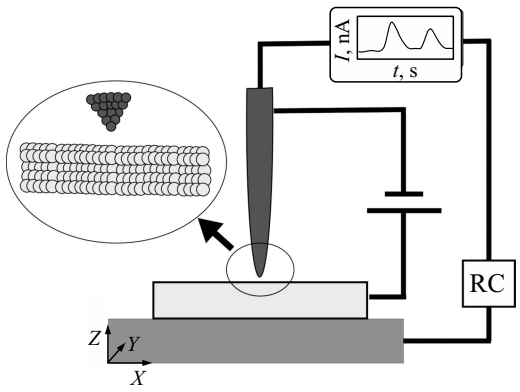

Figure 7. Schematic image of measurements of the I-V curves using the STM (see explanations in the text).

pre-defined numerical control of its motion with respective return coupling (RC), and we energized a circuit between a fixed position of the needle microcontact of the STM and the very sample that was moving by a certain algorithm of motion. Thus, we could carry out the measurements in the local areas with their selected fragmentarily dendritic-clustered structure.

The I-V curves were measured for the eight caverns that were formed after laser impact with the different parameters. Each point on the I-V curve dependence corresponds to its condition of origination of the dendrites

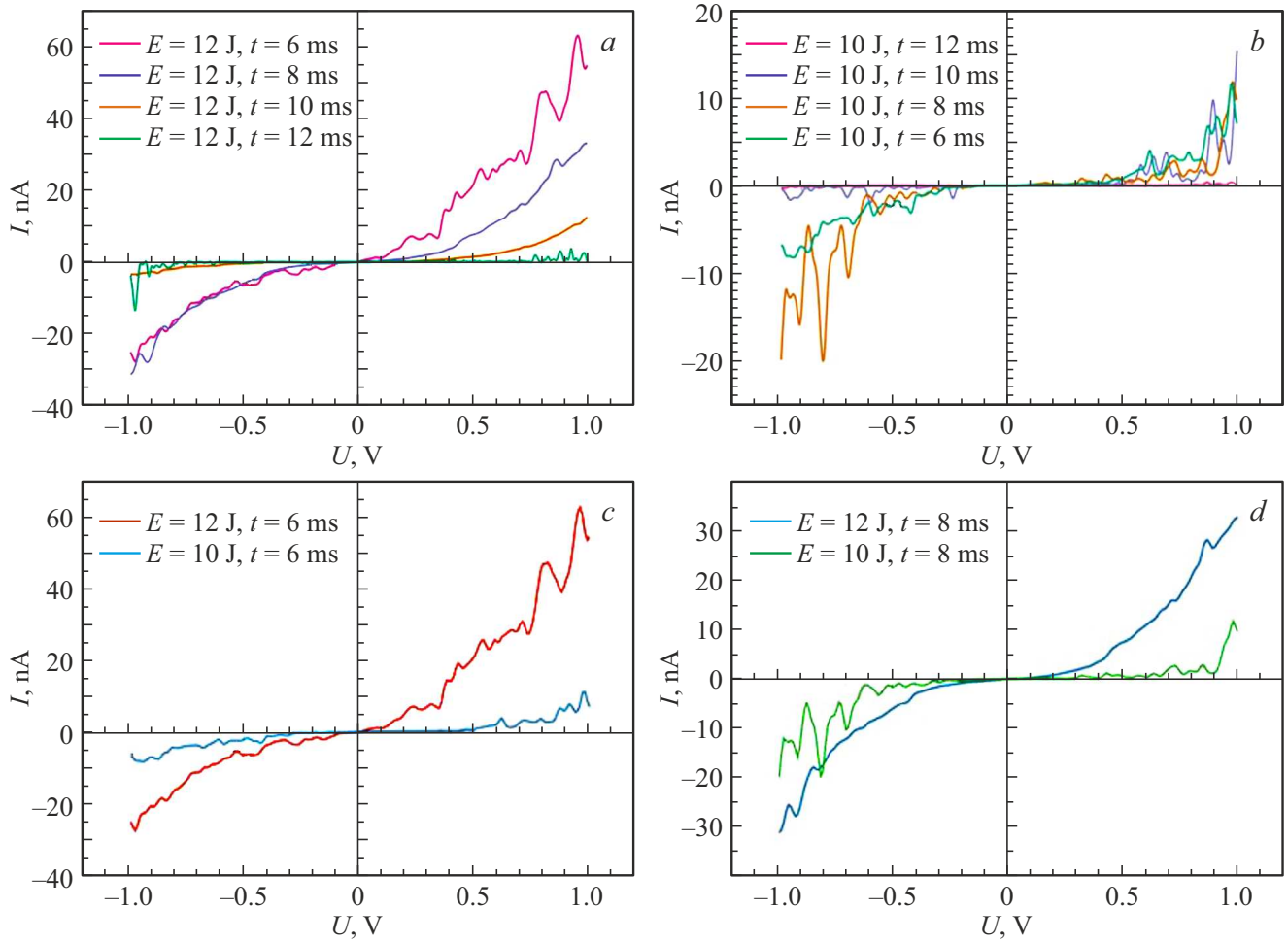

Figure 8. Graph of the dependence of the I-V curves of the dendritic microstructures formed at the constant energy of affecting laser radiation, which is 12 and 10 J for the different cases and at specified different durations of the laser pulses t (marked with a different color): *a*) when $t = 6$ ms; *b*) when $t = 8$ ms; *c*) when $t = 10$ ms; *d*) when $t = 12$ ms.

in terms of energy and duration of laser pulse radiation affecting the sample surface.

The below results for the I-V curves are determined by a dendrite height map that is experimentally obtained under laser impact on the sample with values of vertical heights (the axis $0Z$) up to 1 μm. The dendrites themselves in this dendrite matrix on the sample surface were recorded using the STM in the area of scanning over the surface (the axes X, Y), which had the size of up to 1 mm with an increment of energizing between a contact probe and a displacing sample surface, which was 1 μm (100 points).

All the obtained I-V curves demonstrated a pronounced deviation from the ohmic behavior. Figure 8 shows the graphs of the I-V curves, which display the dependences when varying the laser pulse duration at the fixed energy of laser impact. It is clear that there is a trend of downward variation of the slope angle of the I-V curve dependence with the higher duration of laser impact. It can indicate that the oxide film on the sample surface increases to result in an increase of a value of electrical resistance. Besides, it is clear that values of currents at the impact's laser energy of 12 J for the surface-formed dendrites are higher than for the dendrites produced at the laser energy of 10 J.

It has been also experimentally obtained that at the constant duration of the laser pulse and an increase of the laser radiation energy the I-V curve dependence demonstrates a decrease of electrical resistance of these dendritic structures. This trend remained constant irrespective of the laser pulse duration (Figure 8), but at the same time only the slope angle for the measured dependence of the current value is changed at certain voltage, i. e. a value of differential resistance is changed.

In our considered heterogeneous structures, a relation between voltage and current is described by a non-linear I-V curve, i. e. electrical resistance has not a constant value. Based on the I-V curves, for each point we have calculated static and differential resistance, wherein static resistance is a ratio of voltage to current in a specific point, and differential resistance is defined by a ratio of a small increment of voltage to a small increment of current in

Table 3. Estimated maximum and minimum values of static resistance R_{stat} and differential resistance r_{diff} for the energy E of the laser pulse of duration of t. The data for maximum current I_{max} are given.

E, J	t, ms	I_{max}, mA	$R_{stat_{min}}$, MΩ	$R_{stat_{max}}$, MΩ	$r_{diff_{min}}$, MΩ	$r_{diff_{max}}$, MΩ
12	6	66.94	15.0	970	−3.5	+1.7
12	8	33.41	29.7	750	−1.2	+2.2
12	10	12.78	78.2	1000	−2.5	+3.0
12	12	3.65	300.5	6000	−5.1	+5.1
10	6	15.14	65.8	600	−4.1	+4.1
10	8	16.57	60.3	900	−3.9	+6.0
10	10	20.76	48.2	800	−4.0	+2.7
10	12	0.45	2200	40000	−39.6	+1.5

a selected point, and it can be negative at the non-linear dependence of the I-V curve; it is manifested in solid-state electrical engineering in diode systems of the various type.

Table 3 shows estimated variations of the maximum and minimum values of static and differential resistance on the sample surface with the dendritic structures in various local areas of a map of their distribution over the sample surface, which are formed at the various parameters of laser impact.

The value of I_{max} was selected as the highest one among all the current values measured in the local areas/points on the dendritic surface at the various voltages. The respective voltage was taken from the same array of data along the surface points, as was the maximum current.

In particular, when the laser energy of surface irradiation is 12 J, there is the least static resistance of about 15 MΩ with the short duration of the laser pulse being 6 ms. But, for example, when $t = 12$ ms and at the same laser energy of 12 J the resistance increases to 6000 MΩ, i.e the sample surface becomes almost non-conducting.

When the laser energy is 10 J and the duration of the laser pulse is 12 ms, the highest static resistance is realized — up to 40 GΩ, so is the highest negative differential resistance, −39.6 MΩ. But with a decrease of the pulse duration, resistance of the local areas with the dendrites also decreases.

It enables controlling these electrophysical characteristics in respective problems for various applications.

Parameters of laser impact on the sample, such as the energy of the pulse and its duration, determine fundamental properties of conductance of the configurations of the dendritic structures formed on the sample surface. Thus, when the duration of the laser pulse increases at the energy of 12 J, the static conductance drops from the maximum level's value of 66.7 nS (when the duration of the affecting laser pulse $t = 6$ ms) to the value of 3.3 nS (when the duration

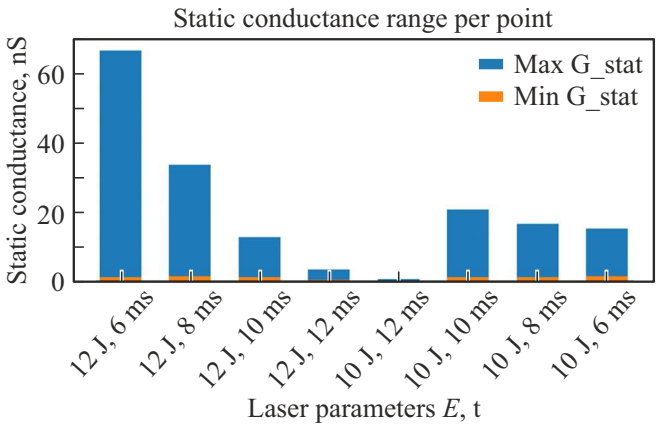

Figure 9. Diagram of variation of static conductance in a dependence on the laser radiation parameters specified on the abscissa axis (the energy E and the duration of the laser pulses t).

of the laser pulse $t = 12$ ms). Reduction of the energy to 10 J results in significant reduction of conductance — when $t = 12$ ms, to the value below 2 nS. However, with reduction of the duration of the laser pulse, there is a slight increase of conductance — within 1.11−1.52 nS.

A respective diagram of variation of static conductance, which is obtained by our data, is shown in Figure 9.

Thus, we have demonstrated that it is possible to controllably vary a map of conductance on the surface of the solid sample for the surface dendritic structures of a various configuration, which are synthesized in the laser experiment. It allows finding schematics solutions required in electrophysics and can be used, for example, for applying new physical principles to develop surface solid-state micro-nanoelectronics of the next generation based on laser-formed topological structures of a pre-defined configuration.

It should be specially emphasized that the very values of local electric fields in the peaks of the dendritic structures can exceed their values for bulk samples of the same composition (cf. [6]) by orders of a magnitude. Therefore, controlling a specific configuration of the dendrites and a shape of their apexes plays a fundamental role and can be regulated exactly in a required way in the laser experiment with taking into account a cross section of the used microcontact.

It is confirmed by results that are obtained in our experiments for several solid-state materials (cf. [5,30]).

At the different rates of heating and cooling the material in the laser experiment, a behavior of the topological geometrical dendritic parameter α that defines a distance between the dendrites over the surface is considerably different for the different materials. At the same time, we experimentally achieve a sharp decrease of the value of α (in tens of times) at a selected rate of non-equilibrium cooling and/or realize almost a plateau for the parameter α in the different conditions of laser impact (cf. [14,31]). Firstly, it is a procedure of producing topological insulators with

micro-nanoscale structures and, secondly, it can exemplify electroschematics solutions in electrophysics of these laser-synthesized structures of a different elemental composition.

Here, particular importance is paid to a structure of electron states, which is varied in a dependence on a surface topology of the solid sample, and to interrelation of charge carriers — electrons. Their certain modified quantum states can result in superconductivity (cf. [32]), in particular, in a wide class of metal-carbon and diamond-like compounds (cf. [6]).

5. Conclusion

We have experimentally studied and simulated fractal structures as per the topological micro-nanostructures that are synthesized on the solid-body surface and have dendrites with their controlled configuration in the laser experiment for the samples made of the AISI 304 stainless steel. It can be presented as an example of the high-entropy compound with a percentage of the elements, which depends on applied laser impact. Raman scattering spectroscopy was used to determine the elemental composition of the synthesized surface structures and to estimate values of mixing entropy for the studied medium in the different conditions. At the same time, the physics of the occurring phenomena can be presented as non-equilibrium laser thermodynamics for the solid body.

It is shown that in the experiments with two-pulse laser ablation for the studied samples of the various type, at different modes of impact by laser radiation with a certain energy in the pulse and its certain duration, the fractal dimension of the formed high-entropy dendrites is 1.9 on average and can be regulated in the required ranges.

For electrophysics in such configurations of the dendrite structures, we have obtained experimental dependences of the current-voltage characteristics (I-V curves) using near-field tunneling microscopy with recording images of the map of the structures that are synthesized on the surface of the solid-state sample. It is demonstrated that resistance, conductance and the I-V curves depend on several factors: on the size of the formed fractal structures, their arrangement on the surface and the chemical composition of the high-entropy alloy, which varies under laser impact, as well as on the degree of roughness of the surface of the target substrate in the experiment. It determines a number of thermophysical phase transformations that are induced in such topological objects under impact of laser radiation and exactly affect the functional characteristics of the studied objects. At the same time, high local conductance can be in certain areas on the surface with the laser-synthesized dendrites for this kind of the topological phase states with controlled non-linear characteristics at the room temeperature of the environment.

These dendritic-fractal structures of the high-entropy alloys with various classes of crystal lattices at phase transformations, which are synthesized in a regulated way during the laser experiment, have both fundamental and applied significance for developing elements and systems of nanophotonics, micro- and nano-electronics on the new physical principles using the topological surface structures of the various configurations.

Conflict of interest

The authors declare that they have no conflict of interest.

References

[1] V.P. Ponomarenko, V.S. Popov, S.V. Popov, E.L. Chepurnov. Adv. Appl. Phys. **7**, *1*, 10 (2019).
[2] V.D. Okunev, Z.A. Samoilenko, Yu.M. Nikolaenko, T.A. D'yachenko, V.V. Burkhovetskii, A.S. Korneevets. FTT **67**, *1*, 90 (2025). (in Russian).
[3] E.N. Mokhov, S.S. Nagalyuk, O.P. Kazarova, S.I. Dorozhkin, V.A. Soltamov. FTT **67**, *1*, 114 (2025). (in Russian).
[4] V.F. Gantmakher. Elektrony v neuporyadochennykh sredakh. Fizmatlit, M. (2013). 288 s. (in Russian).
[5] S.M. Arakelyan, A.O. Kucherik, V.G. Prokoshev, V.G. Rau, A.G. Sergeev. Vvedenie v femtonanofotoniku. Fundamental'nye osnovy i lazernye metody upravlyaemogo polucheniya i diagnostiki nanostrukturirovannykh materialov / Pod red. S.M. Arakelyana. Logos, M. (2020). 744 s. (in Russian).
[6] S.V. Garnov, D.V. Abramov, D.N. Bukharov, T.A. Khudaiberganov, K.S. Khor'kov, A.V. Osipov, S.V. Zhirnova, A.O. Kucherik, S.M. Arakelyan. Phys. — Uspekhi **67**, *2*, 109 (2024).
[7] I.A. Sukhov, A.V. Simakin, G.A. Shafeev, G. Viau, C. Garcia. Quantum Electronics **42**, *5*, 453 (2012).
[8] G. Yang. Laser Ablation in Liquids. Jenny Stanford Publishing, New York (2012). 1192 p.
[9] D.V. Abramov, S.M. Arakelyan, A.F. Galkin, L.D. Kvacheva, I.I. Klimovskiĭ, M.A. Kononov, L.A. Mikhalitsyn, A.O. Kucherik, V.G. Prokoshev, V.V. Savranskiĭ. JETP Lett. **84**, *5*, 258 (2006).
[10] M.C. Downer, H. Ahn, D.H. Reitze, X.Y. Wang. Int. J. Thermophys **14**, *3*, 361 (1993).
[11] N.A. Torkhov. Semiconductors **53**, *1*, 28 (2019).
[12] Z.D. Kvon, D.A. Kozlov, E.B. Olshanetsky, G.M. Gusev, N.N. Mikhailov, S.A. Dvoretsky. Phys. — Uspekhi **63**, *7*, 629 (2020).
[13] M.P. Aleshin, D.D. Tumarkina, E.S. Oparin, D.N. Bukharov, O.Ya. Butkovsky, S.M. Arakelian. Phys. Metals. Metallogr. **125**, *9*, 970 (2024).
[14] D. Bukharov, D. Tumarkina, A. Kucherik, A. Tkachev, S. Arakelyan, I. Burakova, A. Burakov. J. Adv. Mater. Technol. **9**, *3*, 207 (2024).
[15] D.D. Tumarkina, O.Ya. Butkovskii, A.V. Bolachkov, A.A. Burtsev. Fiziko-khimicheskie aspekty izucheniya klasterov, nanostruktur i nanomaterialov *15*, 869 (2023). (in Russian).
[16] A.S. Rogachev. Phys. Metals. Metallogr. **121**, *8*, 733 (2020).
[17] A.N. Maznichevskii, R.V. Sprikut, Y.N. Goikhenberg. Phys. Metals. Metallogr. **122**, *4*, 362 (2021).
[18] L.D. Landau, E.M. Lifshitz. Teoreticheskaya fizika. Elektrodinamika sploshnykh sred. Fizmatlit, M. (2005). (in Russian).
[19] A.A. Abrikosov. Fundamentals of the theory of metals. Dover Publications, New York (2017).

[20] V.V. Sychev. Slozhnye termodinamicheskie sistemy, 5th izd., dop. Izd. dom MEI, M. (2009). 296 s. (in Russian).
[21] K.S. Khorkov, M.Y. Zvyagin, D.A. Kochuev, R.V. Chkalov, S.M. Arakelian, V.G. Prokoshev. Bull. RAS. Phys. **81**, *12*, 1433 (2017).
[22] W.W. Duley. J. Laser Appl. **17**, *1*, 15 (2005).
[23] D.N. Antonov, A.A. Burtsev, O.Ya. Butkovskii. Tech. Phys. **61**, *1*, 108 (2016).
[24] V.P. Dresvyansky, A.V. Kuznetsov, S. Enkbat, E.F. Martynovich,. Bull. RAS. Phys. **84**, *7*, 811 (2020).
[25] L.D. Landau, E.M. Lifshitz. Teoreticheskaya fizika. Fizicheskaya kinetika. Fizmatlit, M. (2002). 536 s. (in Russian).
[26] I.V. Belen'kaya, M.P. Popov, I.A. Starkov, O.A. Savinskaya, S.F. Bychkov, A.P. Nemudryi. Khimiya v interesakh ustoichivogo razvitiya **22**, *4*, 371 (2014). (in Russian).
[27] Integrated database of Raman spectra RRUFF [Electronic source]. URL: https://rruff.info (date of access March 28, 2025).
[28] S.M. Reda. Int. J. Nano Sci. Technol. **1**, *5*, 17 (2013).
[29] D.V. Abramov, O.V. Danilov, D.S. Kitkov, K.S. Khorkov, A.S. Chernikov, S.M. Arakelyan. Tech. Phys. **94**, *2*, 244 (2024).
[30] D.N. Bukharov, V.D. Samyshkin, A.F. Lelekova, D.A. Bodunov, T.V. Kononenko, S.M. Arakelyan, A.O. Kucherik. South-Siberian Scientific Bull. **58**, *6*, 63 (2024).
[31] K.S. Khorkov, V.G. Prokoshev, S.M. Arakelian. J. Adv. Mater. Technol. **6**, *2*, 101 (2021).
[32] V.Z. Kresin, Yu.N. Ovchinnikov. Phys. — Uspekhi **51**, *5*, 427 (2008).

Translated by M.Shevelev